Annals of Medicine

ISSN: 0785-3890 (Print) 1365-2060 (Online) Journal homepage: www.tandfonline.com/journals/iann20

Pulmonary and cerebral damage in COVID-19 survivors: is there any association?

Alberto Arrigoni, Serena Capelli, Gianluca Imeri, Francesca Pennati, Serena Venturelli, Pietro Andrea Bonaffini, Francesco Sanvito, Paolo Marra, Andrea Aliverti, Fabiano Di Marco, Simonetta Gerevini & Anna Caroli

To cite this article: Alberto Arrigoni, Serena Capelli, Gianluca Imeri, Francesca Pennati, Serena Venturelli, Pietro Andrea Bonaffini, Francesco Sanvito, Paolo Marra, Andrea Aliverti, Fabiano Di Marco, Simonetta Gerevini & Anna Caroli (2026) Pulmonary and cerebral damage in COVID-19 survivors: is there any association?, Annals of Medicine, 58:1, 2685416, DOI: 10.1080/07853890.2026.2685416

To link to this article: https://doi.org/10.1080/07853890.2026.2685416

ANNALS OF MEDICINE
2026, VOL. 58, NO. 1, 2685416
https://doi.org/10.1080/07853890.2026.2685416

RESEARCH ARTICLE

OPEN ACCESS Check for updates

Pulmonary and cerebral damage in COVID-19 survivors: is there any association?

Alberto Arrigoni[a#], Serena Capelli[a#], Gianluca Imeri[b], Francesca Pennati[c], Serena Venturelli[d], Pietro Andrea Bonaffini[e,f], Francesco Sanvito[g], Paolo Marra[e,f], Andrea Aliverti[c], Fabiano Di Marco[b], Simonetta Gerevini[h] and Anna Caroli[a]

[a]Bioengineering Department, Istituto di Ricerche Farmacologiche Mario Negri IRCCS, Ranica, BG, Italy; [b]Respiratory Unit, ASST Papa Giovanni XXIII, Bergamo, BG, Italy; [c]Dipartimento di Elettronica, Informazione e Bioingegneria, Politecnico di Milano, Milano, MI, Italy; [d]Infectious Diseases Unit, ASST Papa Giovanni XXIII, Bergamo, BG, Italy; [e]Department of Radiology, ASST Papa Giovanni XXIII, Bergamo, BG, Italy; [f]Department of Medicine and Surgery, University of Milano-Bicocca, Milan, Italy; [g]Department of Radiological Sciences, David Geffen School of Medicine, University of California Los Angeles, Los Angeles, CA, USA; [h]Department of Neuroradiology, ASST Papa Giovanni XXIII, Bergamo, BG, Italy

ABSTRACT

Background: COVID-19 primarily affects the respiratory system, with pulmonary function tests (PFTs) evaluating respiratory impairments and chest CT imaging revealing structural lung abnormalities. However, the disease's multisystem impact – including vascular dysfunction and neurological complications associated with MRI neuroimaging alterations – raises the possibility of shared mechanisms underlying both pulmonary and cerebral involvement, potentially mediated by vascular damage.

Materials and Methods: The study included 27 consecutive COVID-19 patients (median age 59.0 [IQR 50.5 – 70.0] years, 37% female) presenting with concurrent respiratory and neurological symptoms. All patients underwent PFTs, chest CT, and brain MRI. CT images were processed to quantify lung parenchyma, airways, and vasculature, including small-vessel volume (SVV) and air-to-perfusion ratio (APR). Brain MRI analysis assessed gray matter (GM) integrity (volume and cortical thickness), white matter (WM) diffusion metrics (Apparent Diffusion Coefficient, ADC), and GM perfusion (cerebral blood volume, CBV; cerebral blood flow, CBF). Relationships between pulmonary and cerebral metrics were explored using Spearman correlations and multivariable linear regression.

Results: GM volume was positively associated with diffusing capacity for carbon monoxide (DLCO), and cortical thickness was positively associated with alveolar volume (VA). No associations were observed for WM ADC. In contrast, lower pulmonary function (DLCO, VA, forced expiratory volume in 1 s (FEV1), and forced vital capacity (FVC)) were associated with higher GM perfusion.

Conclusions: COVID-19-related pulmonary impairment is associated with reduced GM structural integrity and altered cerebral perfusion, suggesting a lung-brain interplay potentially driven by systemic vascular dysfunction and adaptive cerebrovascular mechanisms. These findings underscore the importance of integrated pulmonary and neurological assessment in post-COVID-19 patients and highlight the need for longitudinal studies to clarify the evolution and clinical consequences of these alterations.

ARTICLE HISTORY
Received 18 March 2026
Accepted 3 June 2026

KEYWORDS
COVID-19; Pulmonary function tests; Chest CT; Brain MRI; Vascular dysfunction; Lung–brain axis

CONTACT Anna Caroli anna.caroli@marionegri.it Bioengineering Department, Istituto di Ricerche Farmacologiche Mario Negri IRCCS, Via G.B. Camozzi 3, Ranica (BG) 24020, Italy
[#]These authors contributed equally to this work.

Supplemental data for this article can be accessed online at https://doi.org/10.1080/07853890.2026.2685416.

GRAPHICAL ABSTRACT

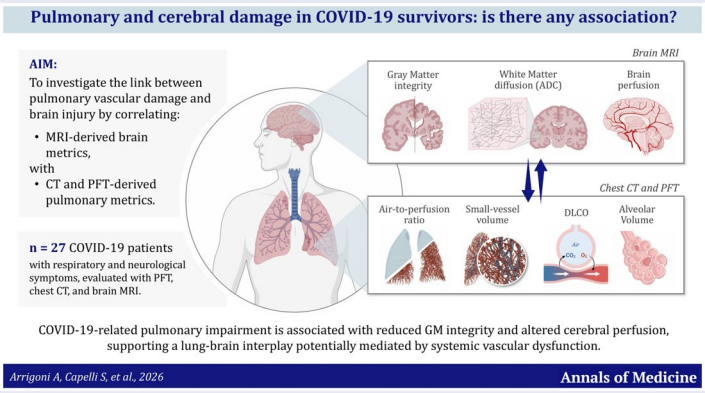

KEY MESSAGES

1. COVID-19-related pulmonary impairment, particularly reduced gas-exchange efficiency, is associated with alterations in brain gray matter structure, including reduced volume and cortical thinning.
2. Gray matter hyperperfusion, reflected by increased CBV and CBF, may reflect cerebrovascular dysregulation linked to systemic vascular and inflammatory injury in COVID-19 patients.
3. These findings highlight a potential brain-lung interplay in COVID-19, underscoring the need for longitudinal studies to assess the evolution and clinical implications of these alterations.

Introduction

The coronavirus disease 2019 (COVID-19), caused by the severe acute respiratory syndrome coronavirus 2 (SARS-CoV-2), emerged as a global health crisis with heterogeneous clinical manifestations. The respiratory system represents the primary target of SARS-CoV-2 infection, with the virus predominantly affecting the airways and lungs [1].

Pulmonary function tests (PFTs) proved to be essential in clinically evaluating pulmonary function impairments in COVID-19 patients [1–3]. Standard PFTs include forced vital capacity (FVC), forced expiratory volume in the first second (FEV1), and the FEV1/FVC, which together assess ventilatory function and airflow obstruction. Alveolar volume (VA) reflects the volume of gas participating in gas exchange, whereas the diffusing capacity for carbon monoxide (DLCO) evaluates the efficiency of gas transfer across the alveolar-capillary membrane. The carbon monoxide transfer coefficient (KCO) further normalizes DLCO for VA, providing an index of gas transfer efficiency.

Alongside PFTs, chest computed tomography (CT) has been pivotal for detecting and monitoring COVID-19-related lung abnormalities, including ground-glass opacities, consolidations, reticulations, and other structural alterations reflecting inflammatory or fibrotic processes [2,3]. Beyond parenchymal injury patterns, CT also provides insights into airway and vascular structures, revealing bronchial dilation or stenosis and alterations in pulmonary vessel morphology [4–6].

A growing body of evidence points to the pulmonary vasculature as a central site of COVID-19 injury. SARS-CoV-2 triggers endothelial inflammation (endotheliitis) *via* ACE2 receptors, followed by thrombosis and angiogenesis—a pattern distinct from other respiratory infections such as influenza. In this context, the immune response plays a pivotal role in fostering inflammation and coagulopathy through cytokine release (e.g., interleukin-1β, interleukin-6 and tumor necrosis factor) and complement activation [7–9]. These mechanisms induce microangiopathy, hypoxemia, and impaired gas exchange [7,9–11].

A vascular pattern of impaired gas exchange is supported by findings from Imeri et al. [12] who compared the DLCO with the diffusing capacity of the lung for nitric oxide (DLNO). Since DLNO primarily reflects membrane conductance rather than the blood flow component, the observed increase in the

DLNO/DLCO ratio suggested a major vascular contribution to the impairment. Additional imaging studies have also described vascular enlargement, mosaic perfusion patterns, and intussusceptive angiogenesis as distinctive pulmonary findings in COVID-19 [10,13,14].

Although COVID-19 primarily affects the lungs, its systemic impact extends to multiple organs, including the heart, kidneys, liver, and nervous system. These multisystem manifestations are thought to be driven largely by systemic inflammation, endothelial dysfunction, and microvascular injury [15].

Moreover, as the pandemic progressed, many patients reported persistent symptoms after the acute phase of infection, a condition now known as 'Long COVID' or post-acute sequelae of SARS-CoV-2 infection (PASC). Characterized by a wide range of symptoms involving multiple organ systems, Long COVID further highlights the systemic nature of the disease. Among the most frequently reported neurological manifestations are olfactory disorders, cognitive impairment ('brain fog'), and psychological distress [16].

In this context, brain Magnetic Resonance Imaging (MRI) has become a key tool for investigating the neurological consequences of COVID-19 [17]. Structural sequences, such as T1-weighted imaging, enable the assessment of cortical and subcortical atrophy and tissue volume changes, while susceptibility-weighted imaging (SWI) is sensitive to cerebral microbleeds (CMBs). Diffusion-weighted imaging (DWI) allows the evaluation of microstructural tissue integrity, and perfusion techniques such as dynamic susceptibility contrast (DSC) MRI provide quantitative measures of cerebral hemodynamics, including Cerebral Blood Flow (CBF) and Cerebral Blood Volume (CBV). Together, these techniques enable a comprehensive assessment of structural, microstructural, and vascular brain alterations associated with COVID-19.

In the acute phase of the disease, brain MRI studies have revealed susceptibility abnormalities and cerebrovascular events such as ischemic and hemorrhagic strokes, as well as cerebral microbleeds (CMBs). These findings support the hypothesis that SARS-CoV-2 may induce neuroinflammation and affect the cerebral vasculature [18–21]. Evidence of perfusion abnormalities further underscores the vascular system as a central site of COVID-19-related injury [19,22,23]. In patients with Long COVID, MRI studies have reported structural and microstructural alterations associated with persistent neurological symptoms. Reductions in gray matter (GM) volume and cortical thickness have been described, and DWI studies demonstrated alterations in the microstructural integrity of brain tissue, along with disruptions in brain connectivity [24–28].

In light of these findings, it is crucial to investigate the potential shared mechanisms underlying COVID-19-related damage to both the pulmonary and central nervous systems, considering the vascular system as a potential driver. Specifically, this study aims to explore the association between pulmonary vascular damage and cerebral injury. To address this, we assessed the correlations between PFTs—particularly DLCO and VA—and structural lung abnormalities derived from chest CT processing, with neuroimaging markers obtained from brain MRI analysis, including GM volume, cortical thickness, White Matter (WM) Apparent Diffusion Coefficient (ADC), and GM perfusion (CBF and CBV). By investigating these interrelationships, this study aims to provide a deeper understanding of the systemic nature of COVID-19 and the association between brain and lung damage.

Materials and methods

Figure 1 summarizes the study design, highlighting the diagnostic tools and key parameters analyzed to investigate these systemic interactions.

Study population

Patients were retrospectively included in the study, representing all COVID-19 cases with available PFTs and who underwent chest CT and brain MRI examinations between March 2020 and October 2021 at ASST Papa Giovanni XXIII in Bergamo, Italy. The data were retrospectively collected and analyzed from May 2024, following approval of the study protocol.

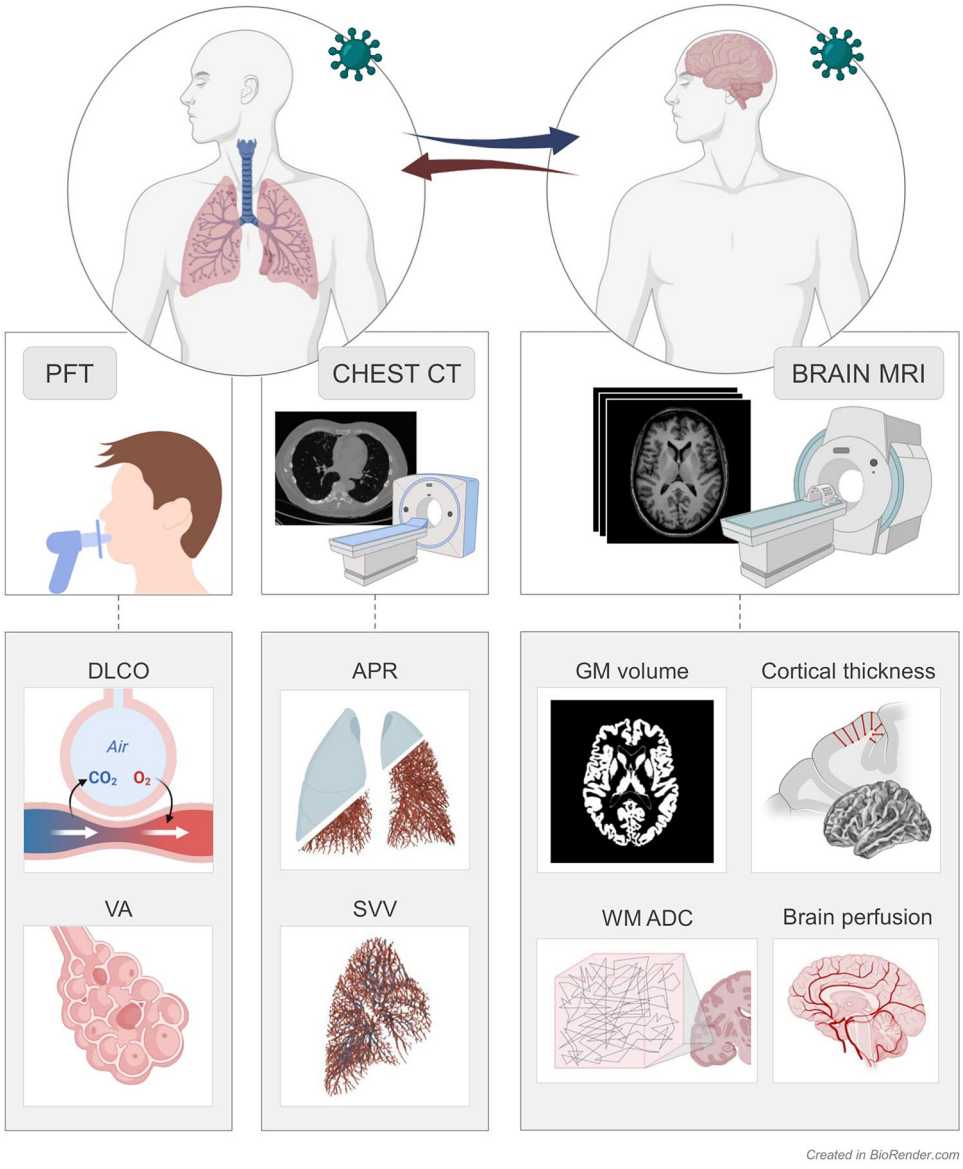

Figure 1. Schematic representation of the study design. The figure illustrates the two main domains of the study—lungs and brain—and the associated diagnostic tests and quantitative measures used to assess pulmonary and cerebral damage in COVID-19 patients. Pulmonary function was evaluated through PFT (DLCO and VA), while structural lung measures (APR and SVV) were assessed through chest CT processing. Brain integrity was evaluated with brain MRI, measuring GM volume, cortical thickness, WM ADC, and perfusion metrics from DSC-MRI.
ADC: Apparent Diffusion Coefficient; APR: Air-to-Perfusion Ratio; DLCO: Diffusing Capacity for Carbon Monoxide; GM: Gray Matter; MRI: Magnetic Resonance Imaging; PFT: Pulmonary Function Test; SVV: Small Vessels Volume; VA: Alveolar Volume; WM: White Matter.

Adult male and female patients (age ≥18 years) were eligible for inclusion if they met the following conditions:

- A documented history of SARS-CoV-2 infection;
- At least one non-contrast enhanced CT scan of the chest and PFTs, conducted after the onset of COVID-19, as part of the follow-up pathway provided for by the 'SURVIVING COVID-19' study (Reg N. 203/20);
- At least one brain MRI examination, including T1-weighted, SWI and DWI scans, motivated by the onset of neurological symptoms after COVID-19 and approved for research use (Reg. 2022-0118).

Patients were excluded in the case of the following:

- A pre-existing pulmonary and/or neurological disorder;
- A suboptimal imaging acquisition affecting processing and analysis.

Figure 2 shows the flow of patient selection.

The study was approved by the *Comitato Etico Territoriale Lombardia 6* of ASST Papa Giovanni XXIII (Approval Number 2023-3.11/481). Written informed consent was obtained from all participants at enrolment, in accordance with the principles of the Declaration of Helsinki.

Clinical and sociodemographic data

Clinical and sociodemographic data were extracted from the patients' electronic medical records contained in the Hospital Information System. The collected data included sociodemographic information such as sex, age, Body Mass Index (BMI), smoking status, and medical history, as well as clinical information regarding symptoms at onset, hospitalization details, and respiratory support received.

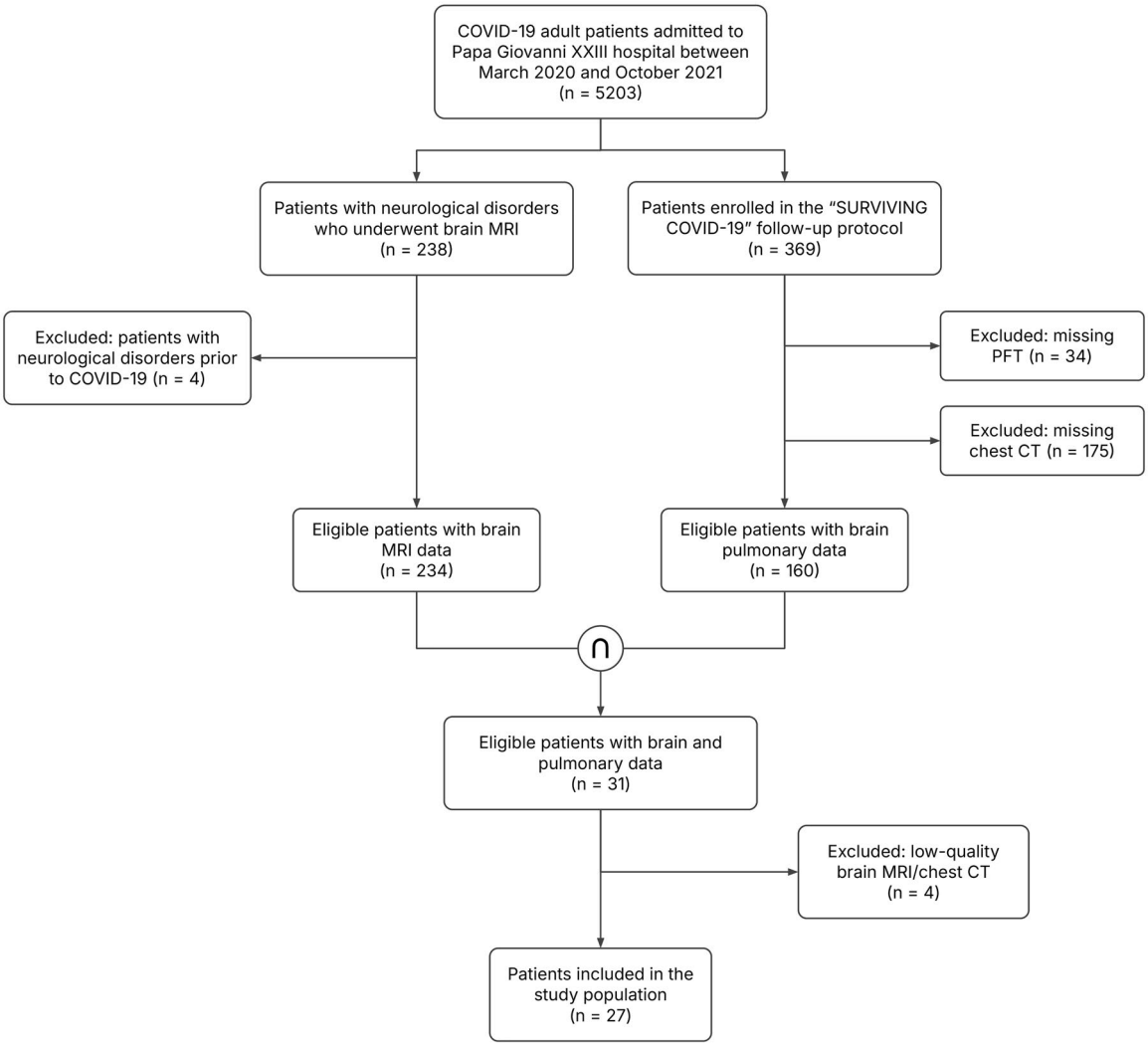

Figure 2. Flowchart illustrating patient selection. The diagram outlines the process of patient inclusion in the study, involving two intersecting cohorts: patients enrolled in the 'Surviving COVID' protocol and patients with COVID-19 who underwent Brain MRI due to neurological disorders.

Pulmonary function tests

The pulmonary assessment included PFTs, which were performed by certified respiratory technicians following contemporary standards [29] and using the Medical Graphics Elite Pro body box with rapid gas analyzers (MGC Diagnostics Corporation, St. Paul, MN, USA). PFT results were interpreted according to current guidelines [30].

The spirometric parameters assessed included FVC, FEV1, the FEV1/FVC ratio, VA, DLCO and KCO. PFT values were reported both as absolute values and as z-scores, which indicate the number of standard deviations a measured PFT value is above or below the predicted normal value. Predicted normal values account for variability in lung function based on age, sex, height, and ethnicity [31].

Chest CT

CT scans acquisition

Chest CT scans were acquired in the supine position during full inspiration, covering the lung bases to the apex, using either a 64-slice or a 16-slice scanner (Brilliance 64 and MX 16-slice, respectively; Philips Medical Systems, Best, Netherlands). All scans were performed without contrast medium and followed a standardized acquisition protocol: tube voltage of 120–140 kVp, automatic exposure control for tube current, pitch of 0.6–1.2, and collimation of 12–40 mm. Images were reconstructed with a slice thickness of 0.5–1.5 mm using sharp kernels and standard lung window settings (width: 1600 HU; level: −600 HU).

CT scans analysis

The image-processing pipeline for chest CT scans was designed to automatically and comprehensively segment and quantify lung structures; full methodological details, including technical validation of the approach, are provided in Arrigoni et al. [32] A manual quality check was also performed to ensure accurate segmentation.

The pipeline starts with the segmentation of the lung parenchyma and the parcellation of individual lobes. Following this stage, it segments the pulmonary airways and vasculature. It also differentiates between well-aerated lung tissue and abnormal regions using Artificial Intelligence (AI), thresholding and region-growing approaches, categorizing the latter into three injury patterns according to density characteristics: reticulation or consolidation, GGOs, and abnormal air-filled spaces (regions devoid of alveolar architecture). Advanced AI tools, specifically publicly available trained U-Net models, perform the initial segmentation of the lungs (https://github.com/JoHof/lungmask), and the preliminary airway segmentation (https://github.com/antonioguj/bronchinet). Vasculature identification is performed using a Jerman 3D vessel enhancement filter [33], binary intensity-based thresholding, and applying context-driven rules leveraging morphological, dimensional, and positional criteria to reduce false positives in the segmentation result. The final vasculature segmentation is additionally categorized into three classes based on vessel radius, computed as the Euclidean distance from the centerline to the boundary:

- Small vessels (radius ≤ 2 mm),
- Medium vessels (radius > 2 mm and ≤ 7 mm),
- Large vessels (radius > 7 mm).

The pipeline application ultimately segmented and quantified the volumes of the key structures and their corresponding classification, including pulmonary vessels, airways, and abnormal lung regions.

Additionally, the total air volume was computed as [34]:

$$\text{Air Volume} = \frac{\text{Tissue Volume} \cdot \text{Mean HU}}{-1000} \tag{1}$$

A coarse air-to-perfusion ratio (APR) was estimated by dividing the air volume by the vasculature volume, offering functional insights derived from structural parameters.

The volumes of segmented regions, including the small vessels volume (SVV), were calculated by counting the voxels within and multiplying the result by the voxel dimensions. These structure volumes were then normalized to the patient-specific total lung volume.

Brain MRI

MRI scans acquisition

All brain MRI scans were acquired at the Neuroradiology Unit of ASST Papa Giovanni XXIII Hospital in Bergamo, Italy, using a 3T General Electric MRI scanner (GE Discovery MR750w; GE Healthcare, Chicago, Illinois, USA).

The MRI acquisition protocol included a T1-weighted multi echo multi planar (MEMP) scan (TE/TR: 9/600 ms; field of view: $250\times250\,mm^2$; matrix: $512\times512\times40$; slice thickness/gap: 3.0/0.4 mm), a SWI axial scan (TE/TR = 26/38 ms; field of view = $240\times240\,mm^2$; matrix: $512\times512\times102$; slice thickness = 1.3 mm), a DSC perfusion scan, and a DWI scan. The DWI scan was acquired axially using a single-shot echo planar imaging sequence (TE/TR: 73/4000 ms; field of view: $240\times240\,mm^2$; matrix: 128×128; slice thickness: 3 mm; b-values: 0 and 1000 s/mm^2; three averaged diffusion encoding directions; NEX = 3; ASSET = 2; fat suppression). The DSC perfusion scan was performed using a T2*-weighted gradient-echo echo-planar imaging (GE-EPI) sequence (TE/TR = 50/2000 ms; field of view: $240\times240\,mm^2$; matrix: 128×128; slice flip angle = 60°; slice thickness/gap = 5.0/0.5 mm; number of slices = 21; temporal resolution = 2 s); A total of 45 dynamic volumes were acquired.

MRI scans analysis

The MRI processing pipelines for the quantitative analysis of T1-weighted and DWI scans were developed internally and have been described in detail in previous publications (see Capelli et al. [24]; Caroli et al. [25]). The processing utilized the following software tools: ImageJ (https://imagej.nih.gov/ij), version 1.53 h; FreeSurfer (https://surfer.nmr.mgh.harvard.edu), version 7.3.0; Statistical Parametric Mapping (The Wellcome Centre for Human Neuroimaging, UCL Queen Square Institute of Neurology, London, UK), version SPM12 (https://www.fil.ion.ucl.ac.uk/spm/software/spm12/); and MATLAB (https://it.mathworks.com/), version: R2020a.

Total Intracranial Volume (TIV) and GM volume were computed from the T1-weighted data using the CAT12 toolbox of SPM. Key preprocessing steps included normalization, bias correction, and skull stripping, followed by tissue classification through probability maps and partial volume estimation. Tissue volumes were calculated by summing voxel probabilities for each tissue type across the brain. For further methodological details, see Tavares et al. [35]. To account for inter-individual differences in brain size, GM volume was normalized dividing it by TIV.

The calculation of mean cortical thickness was performed using FreeSurfer's automated pipeline, which identifies the GM-WM boundary and pial surface to compute the average distance between them across the whole cortex.

For the estimation of the Apparent Diffusion Coefficient (ADC) from DWI scans, the T1-weighted image was coregistered to the $b=0$ DWI sequence, and tissue probability maps (GM, WM, cerebrospinal fluid (CSF)) were generated alongside a whole brain mask. ADC was computed by voxel-wise fitting of the diffusion-weighted signal using the equation:

$$S(b) = S_0 \cdot e^{-b \cdot ADC} \tag{2}$$

where $S(b)$ represents the signal intensity as a function of the b-value (b), and S_0 is the signal intensity at $b=0$. The resulting ADC maps were then masked using the segmentations to restrict the analysis to GM and WM.

Regarding SWI, experienced neuroradiologists visually inspected the scans and annotated the presence or absence of CMBs as a binary variable, irrespective of their location. For DSC perfusion analysis, motion correction was first performed using FSL v6.0 (https://fsl.fmrib.ox.ac.uk/fsl/docs/) MCFLIRT

function. A 6-degree-of-freedom (DoF) rigid-body transformation was applied, using the mean volume as reference. To minimize baseline signal instabilities at acquisition onset, the first volume was removed. To enable anatomically informed perfusion assessment, T1-weighted images were coregistered to DSC space using ANTs v2.5.1 (https://github.com/ANTsX/ANTs), using rigid (6 DoF) registration with mutual information and linear interpolation.

Motion-corrected DSC data were then processed in MATLAB using a modified version of the Dynamic Susceptibility Contrast MRI Toolbox (https://github.com/FAIR-Unipd/dsc-mri-toolbox) [36], which provides semi-automated AIF selection *via* hierarchical clustering, multiple deconvolution approaches for residue function estimation (e.g., SVD variants, nonlinear stochastic regularization, stable spline), and contrast-agent leakage correction implemented following the approach proposed by Boxerman et al. [37].

Statistical analysis

Statistical analyses were performed to explore the relationships between functional and structural pulmonary variables (derived from PFTs and chest CT processing, respectively), and neurological variables obtained from brain MRI processing (normalized GM volume, mean cortical thickness, median WM ADC, and perfusion metrics from DSC-MR). Given the limited size of the dataset and the research hypothesis, the focus was placed specifically on the following pulmonary variables: DLCO and VA, derived from PFTs, and APR and SVV, obtained from chest CT processing.

Spearman's rank correlation coefficient was used to assess pairwise correlations between each cerebral variable and age, pulmonary variables, and MRI time. Because the outcomes of the regression models were brain imaging variables, the time interval between disease onset and brain MRI acquisition was included as a covariate to account for potential time-dependent changes in cerebral structure and perfusion. Time intervals related to pulmonary function tests and chest CT were not included in the regression models to avoid model overfitting given the limited sample size. To further determine the independent contributions of each variable to the neurological outcomes, multivariable linear regression models were applied. Stepwise regression with bidirectional elimination, based on the Akaike Information Criterion (AIC), was employed to identify the most significant predictors in the multivariate models. In addition, a sensitivity analysis was conducted restricting the cohort to participants evaluated at least 6 months after symptom onset (based on MRI timing), in order to assess the robustness of the findings in a more homogeneous post-acute subgroup.

Variance Inflation Factor (VIF) was computed to assess multicollinearity among the predictor variables, and bootstrap analysis with 1000 iterations was performed as a secondary procedure to assess the stability and robustness of regression estimates.

For the PFTs, z-score values (standardized scores) were used in all statistical analyses, as they represent the current international standard recommended by professional bodies such as the American Thoracic Society (ATS) and the European Respiratory Society (ERS) [38].

Statistical significance was defined as $p < 0.05$. All statistical analyses were performed using R software (version 4.4.1; https://www.r-project.org/).

Results

The final study population comprised 27 patients (median age 59.0 [IQR 50.5 – 70.0] years, 10/27 (37%) females) who presented with a range of symptoms at onset, including respiratory symptoms such as dyspnea and cough, as well as neurological symptoms including cognitive deficit, seizures, anosmia, and headache. Among them, DSC perfusion MRI data was available for 13 patients.

Table 1 presents in detail the sociodemographic and clinical features of the 27 patients included in the study.

Table 2 provides a comprehensive overview of all PFTs, chest CT-derived structural pulmonary variables, and brain MRI-derived neuroimaging variables, including evidence of CMBs from SWI review, detected in 3/27 patients, as well as the time elapsed between COVID-19 onset and each examination

Table 1. Sociodemographic and clinical features of the 27 COVID-19 patients included in the study.

N	27
Sociodemographic characteristics	
Sex, F	10/27 (37%)
Age, years	59.0 [50.5 – 70.0]
BMI*	25.2 [24.4 – 28.7]
BMI > 30	5/25 (20%)
Smoker	0/27 (0%)
Former smoker	8/27 (30%)
Medical history**	
Any	10/21 (48%)
> 2	2/21 (10%)
Diabetes mellitus	1/21 (5%)
Hypertension	3/21 (14%)
Coronary artery disease	3/21 (14%)
Chronic heart failure	3/21 (14%)
Chronic renal failure	6/21 (29%)
COPD	0/21 (0%)
Autoimmune disease	1/21 (5%)
Solid neoplasia	0/21 (0%)
Hematologic neoplasia	0/21 (0%)
Liver cirrhosis	0/21 (0%)
Immunodeficiency	0/21 (0%)
Cerebrovascular disease	1/21 (5%)
Previous heart transplant, yes	1/21 (5%)
Symptoms at onset	
Dyspnoea	20/27 (74%)
Cough	15/27 (56%)
Confusion	5/27 (19%)
Asthenia	11/27 (41%)
Anosmia	8/27 (30%)
Headache	1/27 (4%)
Chest pain	3/27 (11%)
Hospitalization	
Hospitalized, yes	25/27 (93%)
Hospitalization length, days	16.0 [9.75 – 31.50]
ICU	6/27 (22%)
Respiratory support	
None (ambient air)	6/27 (22%)
CPAP	3/27 (11%)
Orotracheal Intubation	6/27 (22%)
Low flow oxygen nasal cannula	4/27 (15%)
Reservoir	5/27 (19%)
Venturi mask	3/27 (11%)

Data are shown as median [IQR] or number/total (%).
*2 missing values.
**6 missing values.
BMI: Body Mass Index; CPAP: Continuous Positive Airway Pressure; COPD: Chronic Obstructive Pulmonary Disease; F: Female; ICU: Intensive Care Unit.

(PFT, chest CT, brain MRI). The distribution of the time intervals between disease onset and each examination is illustrated in Supplementary Figure 1.

A comprehensive overview of all pairwise associations between pulmonary and cerebral variables is reported in Supplementary Figure 2. Following sections report the correlations and multivariable-adjusted associations between pulmonary variables and multiple cerebral targets.

GM volume

A significant negative correlation was observed between age and GM volume ($\rho = -0.60$, $p = 0.003$). Among PFT parameters, z(DLCO) exhibited a significant positive correlation with GM volume ($\rho = 0.58$, $p = 0.004$), as illustrated in Figure 3A, while the correlation with z(VA) showed a positive trend that did not reach statistical significance ($\rho = 0.38$, $p = 0.072$). In contrast, parameters derived from chest CT processing, including APR ($\rho = 0.047$, $p = 0.830$) and SVV ($\rho = -0.039$, $p = 0.860$), demonstrated no significant correlations with GM volume. A non-significant negative correlation was also observed with MRI Time ($\rho = -0.22$, $p = 0.26$).

In the multivariable analysis, the initial model included age, z(DLCO), z(VA), APR, SVV, and the time interval between disease onset and brain MRI acquisition as covariates. A stepwise regression approach

Table 2. PFTs, chest CT and brain MRI data of the 27 COVID-19 patients included in the study.

PFTs	
Onset to PFT time, days	125 [88.5 – 141]
SpO_2, %	98.0 [97.0 – 99.0]
mMRC Dyspnoea Scale	
Grade 0	15/27 (56%)
Grade 1	7/27 (26%)
Grade 2	4/27 (15%)
Grade 3	1/27 (4%)
Grade 4	0/27 (0%)
DLCO, mL/min/mmHg*	21.8 [17.8 – 24.9]
z(DLCO)*	−0.52 [−1.42 – 0.00]
VA, L*	5.61 [4.94 – 6.17]
z(VA)*	−0.20 [−0.83 – 0.67]
KCO, mL/min/mmHg/L*	3.88 [3.37 – 4.44]
z(KCO)*	−0.53 [−1.12 – 0.18]
FVC, L	3.61 [3.24 – 4.36]
z(FVC)	−0.42 [−1.16 – 0.52]
FEV1, L	2.86 [2.46 – 3.42]
z(FEV1)	−0.17 [−0.68 – 0.56]
FEV1/FVC	0.78 [0.61 – 1.02]
z(FEV1/FVC)	0.54 [−0.31 – 0.97]
Chest CT data	
Onset to CT time, days	134 [82.5 – 169.5]
Normalized Volume of pathological lung tissue	0.067 [0.023 – 0.161]
Reticulations and consolidations	0.003 [0.001 – 0.011]
GGOs	0.061 [0.021 – 0.136]
Normalized Volume of airways	0.005 [0.003 – 0.006]
Normalized Volume of pulmonary vasculature	0.034 [0.030 – 0.040]
SVV	0.025 [0.020 – 0.028]
Volume of air in the lungs, mL	3503 [3034 – 3973]
APR	22.31 [19.58 – 26.72]
Airways average diameter, mm	4.14 [3.73 – 4.37]
Brain MRI data	
Onset to MRI time, days	158 [98 – 292]
Normalized GM volume	0.383 [0.349 – 0.340]
Mean cortical thickness, mm*	1.91 [1.80 – 2.14]
Median WM ADC, 10–3 mm2/s**	0.778 [0.757 – 0.801]
CMBs evidence	3/27 (11%)
Median GM CBV#	0.290 [0.265 – 0.356]
Median GM CBF#	0.062 [0.055 – 0.072]

Data are shown as median [IQR] or number/total (%).
*2 missing values.
**1 missing value.
#DSC-derived perfusion parameters (CBV and CBF) are reported in arbitrary units (a.u.) as obtained from the deconvolution pipeline, without absolute scaling to mL/100 g or mL/100 g/min.
ADC: Apparent Diffusion Coefficient; APR: Air-to-Perfusion Ratio; CBF: Cerebral Blood Flow; CBV: Cerebral Blood Volume; DLCO: Diffusing Capacity for Carbon Monoxide; FEV1: Forced Expiratory Volume in the first second; FVC: Forced Vital Capacity; GGOs: Ground-Glass Opacities; GM: Gray Matter; KCO: Carbon Monoxide Transfer Coefficient; PFT: Pulmonary Function Test; SVV: Small Vessels Volume; VA: Alveolar Volume; WM: White Matter.

optimized the model, retaining age, z(DLCO), APR and SVV as predictors. In such a model, age showed a significant negative association (OR, 0.997 [95% CI, 0.996–0.999], $p < 0.001$) and z(DLCO) showed a positive association with GM volume (OR, 1.015 [95% CI, 1.004–1.027]; $p = 0.011$). APR and SVV were included but did not reach significance ($p = 0.078$ and $p = 0.093$, respectively).

VIFs confirmed the absence of significant multicollinearity among predictors (all VIFs < 3.5). Bootstrap analysis supported the robustness of the regression coefficients, with minimal bias and acceptable standard errors. Full statistical details are reported in Supplementary Table 1, while the corresponding coefficient plot of the standardized stepwise model is shown in Supplementary Figure 3A.

Cortical thickness

A negative trend was observed between age and cortical thickness ($\rho = -0.35$, $p = 0.102$), though it did not reach statistical significance. Cortical thickness showed a significant positive correlation with z(VA) ($\rho = 0.43$, $p = 0.043$), as illustrated in Figure 3B. No significant correlations were found between cortical

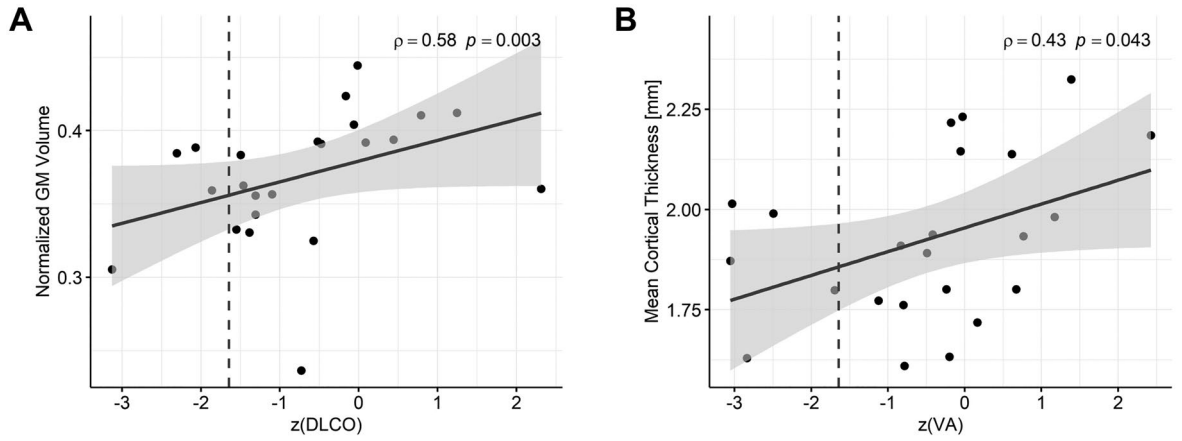

Figure 3. Correlation analysis between pulmonary function and brain structural integrity. (**A**) Linear regression of z(DLCO) on normalized GM volume. (**B**) Linear regression of z(VA) on mean cortical thickness (in mm). Analyses were performed on the available paired dataset ($n = 23$). ρ denotes Spearman's rank correlation coefficient, with the pertinent p-value. The vertical dashed line indicates the lower limit of normality for z(DLCO) and z(VA) (z = −1.645).
DLCO: Diffusing Capacity for Carbon Monoxide; GM: Gray Matter; VA: Alveolar Volume.

thickness and z(DLCO) ($\rho = 0.25$, $p = 0.256$), APR ($\rho = -0.16$, $p = 0.472$), or SVV ($\rho = 0.20$, $p = 0.364$). A significant negative correlation was also observed between MRI Time and cortical thickness ($\rho = -0.51$, $p = 0.010$).

In the final model from multivariable analysis after stepwise optimization, mean cortical thickness showed significant independent associations with age (OR, 0.991 [95% CI, 0.985–0.997]; $p = 0.006$), z(VA) (OR, 1.048 [95% CI, 1.001–1.098]; $p = 0.044$), and MRI time (OR, 0.999 [95% CI, 0.999–1.000]; $p = 0.003$). No other variables were retained in the model.

VIFs confirmed no significant multicollinearity among predictors in the final model (all VIFs < 1.1). Bootstrap analysis confirmed the robustness of the regression coefficients, showing minimal bias and acceptable standard errors. Full statistical details are reported in Supplementary Table 2, while the corresponding coefficient plot of the standardized stepwise model is shown in Supplementary Figure 3B.

GM perfusion

Regarding PFT-derived parameters, GM CBV showed a significant negative correlation with z(FEV1) ($\rho = -0.63$, $p = 0.021$), while negative trends were observed with z(FVC) ($\rho = -0.47$, $p = 0.105$), z(DLCO) ($\rho = -0.41$, $p = 0.164$), and z(VA) ($\rho = -0.44$, $p = 0.155$), none of which reached statistical significance (Figure 4A–D).

For GM CBF, a moderate negative correlation was observed with z(VA), while not reaching statistical significance ($\rho = -0.56$, $p = 0.060$). No significant correlations were found between GM CBF and z(DLCO) ($\rho = -0.32$, $p = 0.279$), z(FEV1) ($\rho = -0.35$, $p = 0.238$), or z(FVC) ($\rho = -0.38$, $p = 0.201$) (Figure 4E–H).

Among CT-derived parameters, SVV showed positive but non-significant correlations with both GM CBV ($\rho = 0.41$, $p = 0.164$) and GM CBF ($\rho = 0.39$, $p = 0.194$).

WM ADC

A moderate positive correlation was observed between age and WM ADC ($\rho = 0.38$, $p = 0.072$), though it did not reach statistical significance. No significant correlations were found between WM ADC and any of the pulmonary parameters, including z(DLCO) ($\rho = -0.20$, $p = 0.366$), z(VA) ($\rho = -0.23$, $p = 0.289$), APR ($\rho = -0.18$, $p = 0.412$), and SVV ($\rho = 0.10$, $p = 0.663$). Furthermore, there was no significant correlation with MRI Time ($\rho = 0.07$, $p = 0.730$).

In the final multivariable model, age, APR, and MRI time were retained as predictors, but none showed significant independent associations with WM ADC ($p = 0.113$, $p = 0.117$, and $p = 0.147$, respectively).

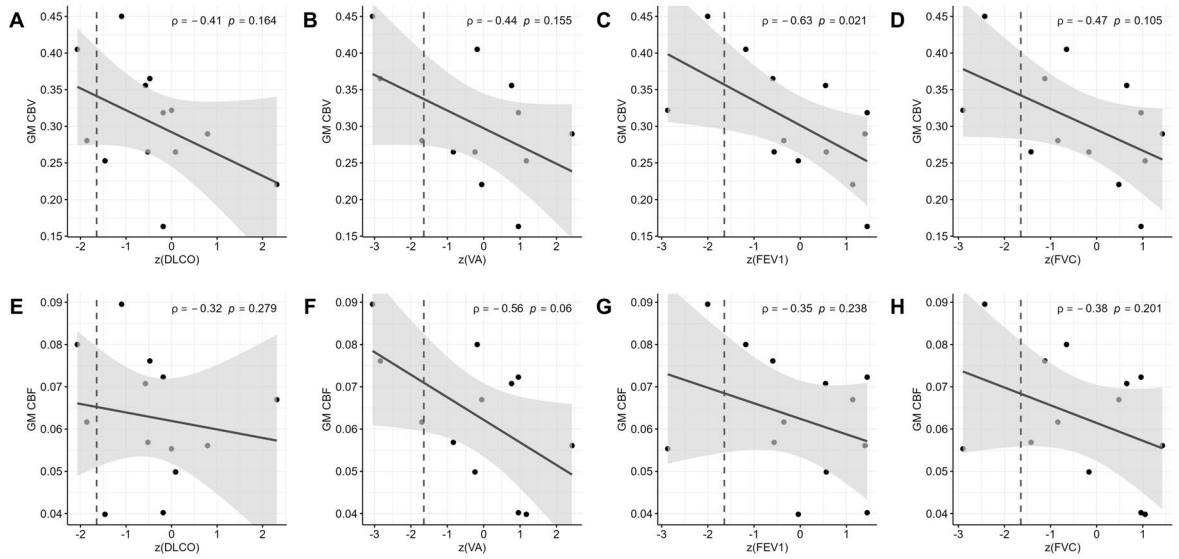

Figure 4. Relationships between GM perfusion parameters and pulmonary function tests. Top row: scatter plots showing correlations between GM CBV and A) z(DLCO), B) z(VA), C) z(FEV1), and D) z(FVC). Bottom row: scatter plots showing correlations between GM CBF and E) z(DLCO), F) z(VA), G) z(FEV1), and H) z(FVC). Analyses were performed on the available paired dataset ($n = 13$). ρ denotes Spearman's rank correlation coefficient, with the pertinent p-value. The vertical dashed line indicates the lower limit of normality for z(DLCO) and z(VA) ($z = -1.645$).
CBF: Cerebral Blood Flow; CBV: Cerebral Blood Volume; DLCO: Diffusing Capacity for Carbon Monoxide; FEV1: Forced Expiratory Volume in the first second; FVC: Forced Vital Capacity.

VIFs confirmed no significant multicollinearity among predictors in the final model (all VIFs < 1.4). Bootstrap analysis confirmed the robustness of the regression coefficients, with minimal bias and acceptable standard errors.

Sensitivity analysis

A sensitivity analysis restricted to patients evaluated ≥6 months after COVID-19 onset (based on MRI timing) confirmed the stability of the associations observed in the full cohort for most neuroimaging markers. The association between cortical thickness and time from onset was attenuated in the restricted analysis, suggesting that the effect may be driven predominantly by early post-acute changes. No meaningful differences were observed for GM volume and WM diffusion metrics.

A further restriction to ≥12 months was not feasible due to limited sample size.

Discussion

This study provides novel insights into the associations between COVID-19-related pulmonary damage and brain integrity by integrating clinically meaningful indicators from both systems. Pulmonary status was assessed through PFT variables (DLCO, VA, FEV1, and FVC), which capture gas exchange efficiency, alveolar volume, and ventilatory/airway function, along with CT-derived structural measures (APR and SVV) reflecting pulmonary vascular involvement and changes in lung aeration/vasculature balance. These pulmonary markers were compared with MRI-derived indicators of brain health, including GM volume and cortical thickness (indices of neuronal integrity), ADC (reflecting WM microstructure), and perfusion metrics such as CBF and CBV (markers of cerebrovascular function). Together, these complementary measures allow us to assess whether residual pulmonary alterations are accompanied by changes in cerebral structure and perfusion, supporting the hypothesis of a shared vascular component in post-COVID-19 multisystem involvement.

A significant negative correlation was observed between age and GM volume, consistent with the well-documented effects of aging on GM integrity [39–41]. This finding supports the inclusion of age as a covariate in the multivariable models to account for its influence on brain integrity and isolate the specific associations between brain and lung markers.

Pulmonary function, particularly the gas-exchange efficiency reflected by z(DLCO), showed a significant positive association with GM volume in both correlation and multivariable analyses. In addition, z(VA) was positively associated with cortical thickness. Taken together, these findings suggest that impaired pulmonary physiology may be associated with reduced gray matter structural integrity. This observation is consistent with the study by Mahammedi et al. [42] who reported that the severity of pulmonary disease in COVID-19 patients could predict acute neuroimaging abnormalities in COVID-19 patients, including white-matter pathology (e.g., leukoencephalopathy and multifocal T2/FLAIR lesions) as well as ischemic or haemorrhagic injury. Given our results and prior knowledge, we suggest that vascular inflammation is a key mechanism linking pulmonary and cerebral findings, with COVID-19 inducing endothelial dysfunction, systemic inflammation, and microvascular damage that could explain the correlations observed between the two districts [15].

Consistently, in our cohort, worse pulmonary physiology (lower z-scores of DLCO, VA, FEV1 and FVC) was associated with GM hyperperfusion (higher CBV and CBF). Similar findings were reported by Staab et al. [43] who similarly reported that reduced pulmonary gas-exchange efficiency was associated with increased cerebral perfusion in Long COVID patients. Although the underlying mechanisms remain uncertain and cannot be determined from the present data, one speculative interpretation is that systemic or vascular hypoxia may elicit cerebrovascular responses aimed at maintaining adequate tissue oxygenation, potentially involving vasodilation and, possibly, angiogenic remodelling. The positive association between GM perfusion (CBV and CBF) and CT-derived SVV observed in our data may be consistent with the presence of a shared vascular phenotype affecting multiple organ systems, though this remains to be confirmed in studies with direct vascular biomarkers.

In this scenario, endothelial dysfunction and microvascular inflammation, which may contribute to DLCO reduction at the lung level, could potentially disrupt the blood-brain barrier (BBB), leading to vasogenic edema in the acute phase of the disease. Concurrently, microvascular dysregulation could promote heterogeneous vasodilation and altered capillary transit times, resulting in higher CBF and CBV while potentially reducing the efficiency of tissue oxygen extraction.

Whether this hyperperfusion reflects a compensatory response to impaired gas exchange or instead represents a marker of inefficient microvascular oxygen delivery cannot be determined from our data and requires further investigation. Over time, the hemodynamic dysregulation and underlying neuroinflammation, could contribute to long-term structural GM loss and cortical thinning [44,45], though longitudinal evidence is needed to test this temporal hypothesis.

The resolution of vasogenic oedema over time is supported by a prior study that examined ADC in a larger dataset of patients with neurological symptoms after COVID-19 and with diverse MRI acquisition timing relative to the onset of the disease [25]. In parallel, the present study observed a significant negative correlation between cortical thickness and the MRI time from the disease onset, suggesting that neuroinflammation and inefficient tissue oxygen delivery secondary to vascular impairment may promote neurodegeneration and GM atrophy in the long term. This potential time-related effect warrants further research in longitudinal studies. To date, no longitudinal studies have quantified cortical thickness across multiple time points following COVID-19 infection [17].

The association between cortical thickness and VA is consistent with similar systemic mechanisms. Processes that impair microvascular health systemically could potentially contribute to reduced cortical thickness in the brain and to lower VA in the lung.

These findings underscore the shared vulnerability of the brain and lungs to systemic vascular and inflammatory injury in COVID-19, providing insight into the interconnected nature of post-COVID-19 complications.

Beyond the vascular framework, it is important to acknowledge that the observed brain structural and perfusion alterations are likely multifactorial, and that our data cannot distinguish between concurrent mechanistic pathways. Neuroinflammation and glial activation—including microglial reactivity and astrocyte-mediated responses triggered by SARS-CoV-2—may independently contribute to GM volume loss and cortical thinning, irrespective of vascular involvement. Brain network dysfunction has also been reported in post-COVID populations [26,27,46] and may underlie some of the structural correlates observed here. Additionally, metabolic and mitochondrial alterations—including impaired neuronal energy metabolism secondary to systemic hypoxia, inflammation, or direct viral effects—represent a

further potential contributor to the GM changes observed [47,48]. These pathways are not mutually exclusive and are likely to interact; disentangling their relative contributions will require multimodal longitudinal studies incorporating inflammatory biomarkers, functional imaging, and metabolic measures.

Our findings differ from those of Chen et al. [49], who observed a correlation between pulmonary function recovery and increased global GM volume in a small case series of four patients followed for 12 months post-recovery. This discrepancy could potentially be influenced by the small sample size, which may affect the generalizability of their observations. Additionally, although Chen et al. observed a significant correlation between pulmonary function and GM volume, the specific statistical methods and metrics used to assess this association were not detailed in their paper, making it difficult to draw direct comparisons with our results.

At the microstructural level, no significant associations were observed between PFTs or chest CT markers and WM ADC. While microstructural and connectivity alterations in WM, as well as vascular-related lesions like CMBs, have been previously reported [21,25,26], this finding may suggest that GM is more vulnerable to the pathophysiological processes driven by the vascular component also affecting the lungs. This vulnerability may be attributed to GM's greater metabolic demand and vascular density. The increased susceptibility to systemic vascular damage, associated tissue hypoxia, and prolonged inflammation could explain the significant correlations observed with GM-related markers and absent with WM ones. In addition, WM alterations may be more subtle and could require more observations and advanced techniques, such as DTI, to detect microstructural alterations potentially associated with pulmonary changes.

Previous studies have consistently reported GM atrophy and cortical thinning in COVID-19 patients compared to healthy controls, primarily in cross-sectional designs [24,26,27,50–54]. While these studies highlight the neurological impact of COVID-19, our findings add specificity by identifying the coexistence between reduced gas exchange efficiency and reduced brain structural integrity.

The literature on lung-brain associations in COVID-19 remains limited, with most prior research focusing on neurological or pulmonary aspects independently rather than investigating their potential interplay. To our knowledge, no prior studies have combined PFTs, chest CT-derived measures, and advanced brain MRI metrics to explore lung-brain relationships in COVID-19, underscoring the novel, integrative framework of this work.

Several limitations should be acknowledged. First, the modest sample size limits generalizability and precluded inclusion of additional clinical variables in regression models due to overfitting risk. However, the dataset's multimodal depth—integrating PFTs, quantitative chest CT, and advanced brain MRI—a unique strength. Given the retrospective nature of the study and the limited sample size, the multivariable analyses are best interpreted as exploratory and hypothesis-generating.

Second, perfusion indices were derived from contrast-based DSC-MRI within a clinical protocol, which may limit standardization and repeatability compared with non-contrast approaches such as ASL. In addition, our hyperperfusion findings should be interpreted in the context of heterogeneous reports of COVID-19 related perfusion abnormalities, with studies showing regional hypoperfusion, and other describing hyperperfusion patterns [43,55]. Future longitudinal studies combining perfusion imaging and additional vascular biomarkers are warranted.

In addition, we relied on global brain metrics rather than region-of-interest analyses. While COVID-19-related neurological involvement is known to preferentially affect specific regions, a region-specific approach would have substantially increased the number of statistical comparisons, requiring correction thresholds that our sample size cannot adequately support. Global metrics were therefore prioritized to preserve statistical robustness. Future studies with larger cohorts should incorporate region-of-interest analyses.

Another limitation relates to the pulmonary profile of the cohort. Most patients exhibited values within the normal physiological range, as assessments occurred ~125 days post-infection, which should be considered when interpreting effect magnitudes.

Furthermore, while varying MRI acquisition times from onset offer insights into the temporal evolution of cerebral alterations, namely the cortical thinning, this variability also adds complexity to the analysis, posing a limitation in interpreting the results. To partially account for this issue, the time interval between disease onset and brain MRI acquisition was included as a covariate in the multivariable regression models, allowing us to control for potential time-dependent changes in cerebral structure and perfusion. However, the limited sample size prevented the inclusion of additional timing variables without

increasing the risk of model overfitting. Future studies with longitudinal designs and synchronized multimodal assessments will be essential to better characterize the temporal dynamics of lung-brain interactions following COVID-19.

Conclusions

By integrating PFTs, chest CT-derived structural variables, and advanced brain MRI metrics, this study provides a novel perspective on the link between COVID-19-related pulmonary damage and neuroanatomical alterations. Our findings demonstrate that pulmonary impairment—particularly reduced gas-exchange efficiency (DLCO) and alveolar volume (VA)—is associated with reduced GM volume, cortical thinning, and GM hyperperfusion. These associations point to a potential role for systemic vascular dysfunction as a common pathway connecting pulmonary and cerebral sequelae. While the observed associations do not imply causation, they underscore the interconnected nature of post-COVID-19 complications and highlight the value of a multidisciplinary, multiparametric approach. Future longitudinal studies in larger cohorts are essential to confirm these patterns and elucidate the underlying mechanisms.

Acknowledgements

A.A. and S.C. would like to express their gratitude to the '*Aiuti per la Ricerca sulle Malattie Rare*' (A.R.M.R.) Foundation for supporting them with a scholarship.

Authors contributions

CRediT: **Alberto Arrigoni**: Conceptualization, Formal analysis, Investigation, Methodology, Software, Visualization, Writing – original draft; **Serena Capelli**: Conceptualization, Formal analysis, Investigation, Methodology, Software, Visualization, Writing – original draft; **Gianluca Imeri**: Data curation, Resources, Validation, Writing – review & editing; **Francesca Pennati**: Conceptualization, Supervision, Validation, Writing – review & editing; **Serena Venturelli**: Data curation, Resources, Validation, Writing – review & editing; **Pietro Andrea Bonaffini**: Data curation, Resources, Validation, Writing – review & editing; **Francesco Sanvito**: Methodology, Validation, Writing – review & editing; **Paolo Marra**: Resources, Validation, Writing – review & editing; **Andrea Aliverti**: Conceptualization, Supervision, Writing – review & editing; **Fabiano Di Marco**: Conceptualization, Supervision, Validation, Writing – review & editing; **Simonetta Gerevini**: Conceptualization, Supervision, Validation, Writing – review & editing; **Anna Caroli**: Conceptualization, Supervision, Writing – review & editing.

Disclosure statement

The authors declare that they have no known competing financial interests or personal relationships that could have appeared to influence the work reported in this paper.

Funding

The study was supported in part by a grant from Brembo SpA (Curno, Bergamo, Italy), under the initiative 'Progetto TrexUno'.

ORCID

Alberto Arrigoni http://orcid.org/0000-0002-1914-6582
Serena Capelli http://orcid.org/0000-0002-8450-3806
Gianluca Imeri http://orcid.org/0000-0003-1139-6509
Francesca Pennati http://orcid.org/0000-0001-8896-8224
Serena Venturelli http://orcid.org/0000-0002-5679-2516
Pietro Andrea Bonaffini http://orcid.org/0000-0001-5335-9429
Francesco Sanvito http://orcid.org/0000-0003-3379-9958
Paolo Marra http://orcid.org/0000-0003-4935-8110
Andrea Aliverti http://orcid.org/0000-0002-2950-0231
Fabiano Di Marco http://orcid.org/0000-0002-1743-0504
Simonetta Gerevini http://orcid.org/0000-0002-2374-194X
Anna Caroli http://orcid.org/0000-0002-4130-4663

Data availability statement

The data that supports the findings of this study are available from the corresponding author, upon reasonable request.

References

[1] Schaefer I-M, Padera RF, Solomon IH, et al. In situ detection of SARS-CoV-2 in lungs and airways of patients with COVID-19. Mod Pathol. 2020;33(11):2104–2114. doi:10.1038/s41379-020-0595-z.

[2] Balbi M, Conti C, Imeri G, et al. Post-discharge chest CT findings and pulmonary function tests in severe COVID-19 patients. Eur J Radiol. 2021;138:109676. doi:10.1016/j.ejrad.2021.109676.

[3] Corsi A, Caroli A, Bonaffini PA, et al. Structural and functional pulmonary assessment in severe COVID-19 survivors at 12 months after discharge. Tomography. 2022;8(5):2588–2603. doi:10.3390/tomography8050216.

[4] Hu Q, Liu Y, Chen C, et al. Reversible bronchiectasis in COVID-19 survivors with acute respiratory distress syndrome: pseudobronchiectasis. Front Med. 2021;8:739857. doi:10.3389/fmed.2021.739857.

[5] Chen L, Tang R, Chen H, et al. Pulmonary vasculature: a target for COVID-19. Am J Respir Crit Care Med. 2021;203(2):260–261. doi:10.1164/rccm.202009-3564LE.

[6] Lins M, Vandevenne J, Thillai M, et al. Assessment of small pulmonary blood vessels in COVID-19 patients using HRCT. Acad Radiol. 2020;27(10):1449–1455. doi:10.1016/j.acra.2020.07.019.

[7] McGonagle D, O'Donnell JS, Sharif K, et al. Immune mechanisms of pulmonary intravascular coagulopathy in COVID-19 pneumonia. Lancet Rheumatol. 2020;2(7):e437–e445. doi:10.1016/S2665-9913(20)30121-1.

[8] Riou M, Coste F, Meyer A, et al. Mechanisms of pulmonary vasculopathy in acute and long-term COVID-19: a review. Int J Mol Sci. 2024;25(9):4941. doi:10.3390/ijms25094941.

[9] Osburn WO, Smith K, Yanek L, et al. Markers of endothelial cell activation are associated with the severity of pulmonary disease in COVID-19. PLoS One. 2022;17(5):e0268296. doi:10.1371/journal.pone.0268296.

[10] Ackermann M, Verleden SE, Kuehnel M, et al. Pulmonary vascular endothelialitis, thrombosis, and angiogenesis in Covid-19. N Engl J Med. 2020;383(2):120–128. doi:10.1056/NEJMoa2015432.

[11] Batah SS, Fabro AT. Pulmonary pathology of ARDS in COVID-19: a pathological review for clinicians. Respir Med. 2021;176:106239. doi:10.1016/j.rmed.2020.106239.

[12] Imeri G, Conti C, Caroli A, et al. Gas exchange abnormalities in Long COVID are driven by the alteration of the vascular component. Multidiscip Respir Med. 2024;19(1):738. doi:10.5826/mrm.2024.938.

[13] Lang M, Som A, Carey D, et al. Pulmonary vascular manifestations of COVID-19 Pneumonia. Radiol Cardiothorac Imaging. 2020;2(3):e200277. doi:10.1148/ryct.2020200277.

[14] Pérez-Mies B, Gómez-Rojo M, Carretero-Barrio I, et al. Pulmonary vascular proliferation in patients with severe COVID-19: an autopsy study. Thorax. 2021;76(10):1044–1046. doi:10.1136/thoraxjnl-2020-216714.

[15] Zhang J, Tecson KM, McCullough PA. Endothelial dysfunction contributes to COVID-19-associated vascular inflammation and coagulopathy. RCM. 2020;21:315–319.

[16] Davis HE, Assaf GS, McCorkell L, et al. Characterizing long COVID in an international cohort: 7 months of symptoms and their impact. EClinicalMedicine. 2021;38:101019. doi:10.1016/j.eclinm.2021.101019.

[17] Mohammadi S, Ghaderi S. Post-COVID-19 conditions: a systematic review on advanced magnetic resonance neuroimaging findings. Neurol Sci. 2024;45(5):1815–1833. doi:10.1007/s10072-024-07427-6.

[18] Klironomos S, Tzortzakakis A, Kits A, et al. Nervous system involvement in Coronavirus Disease 2019: results from a retrospective consecutive neuroimaging cohort. Radiology. 2020;297(3):E324–E334. doi:10.1148/radiol.2020202791.

[19] Boparai MS, Musheyev B, Hou W, et al. Brain MRI findings in severe COVID-19 patients: a meta-analysis. Front Neurol. 2023;14:1258352. doi:10.3389/fneur.2023.1258352.

[20] Uginet M, Breville G, Hofmeister J, et al. Cerebrovascular complications and vessel wall imaging in COVID-19 encephalopathy – A pilot study. Clin Neuroradiol. 2022;32(1):287–293. doi:10.1007/s00062-021-01008-2.

[21] Napolitano A, Arrigoni A, Caroli A, et al. Cerebral microbleeds assessment and quantification in COVID-19 patients with neurological manifestations. Front Neurol. 2022;13:884449. doi:10.3389/fneur.2022.884449.

[22] Mohammadi S, Ghaderi S, Fatehi F. Brain perfusion alterations in patients and survivors of COVID-19 infection using arterial spin labeling: a systematic review. Brain-X. 2024;2(3):e70007. doi:10.1002/brx2.70007.

[23] Manca R, De Marco M, Ince PG, et al. Heterogeneity in regional damage detected by neuroimaging and neuropathological studies in older adults with COVID-19: a cognitive-neuroscience systematic review to inform the long-term impact of the virus on neurocognitive trajectories. Front Aging Neurosci. 2021;13:646908. doi:10.3389/fnagi.2021.646908.

[24] Capelli S, Arrigoni A, Napolitano A, et al. MRI evidence of gray matter loss in COVID-19 patients with cognitive and olfactory disorders. Ann Clin Transl Neurol. 2024;11(9):2457–2472. doi:10.1002/acn3.52164.

[25] Caroli A, Capelli S, Napolitano A, et al. Brain diffusion alterations in patients with COVID-19 pathology and neurological manifestations. Neuroimage Clin. 2023;37:103338. doi:10.1016/j.nicl.2023.103338.

[26] Arrigoni A, Previtali M, Bosticardo S, et al. Brain microstructure and connectivity in COVID-19 patients with olfactory or cognitive impairment. Neuroimage Clin. 2024;43:103631. doi:10.1016/j.nicl.2024.103631.

[27] Douaud G, Lee S, Alfaro-Almagro F, et al. SARS-CoV-2 is associated with changes in brain structure in UK Biobank. Nature. 2022;604(7907):697–707. doi:10.1038/s41586-022-04569-5.
[28] Boito D, Eklund A, Tisell A, et al. MRI with generalized diffusion encoding reveals damaged white matter in patients previously hospitalized for COVID-19 and with persisting symptoms at follow-up. Brain Commun. 2023;5(6):fcad284. doi:10.1093/braincomms/fcad284.
[29] Graham BL, Steenbruggen I, Miller MR, et al. Standardization of Spirometry 2019 Update. An Official American Thoracic Society and European Respiratory Society Technical Statement. Am J Respir Crit Care Med. 2019;200(8):e70–e88. doi:10.1164/rccm.201908-1590ST.
[30] Pellegrino R, Viegi G, Brusasco V, et al. Interpretative strategies for lung function tests. Eur Respir J. 2005;26(5):948–968. doi:10.1183/09031936.05.00035205.
[31] Quanjer PH, Stanojevic S, Cole TJ, et al. Multi-ethnic reference values for spirometry for the 3–95-yr age range: the global lung function 2012 equations. Eur Respir J. 2012;40(6):1324–1343. doi:10.1183/09031936.00080312.
[32] Arrigoni A, Pennati F, Bonaffini PA, et al. Advanced lung segmentation on chest HRCT: comprehensive pipeline for quantification of airways, vessels, and injury patterns. Radiol Med. 2026;131(4):634–647. doi:10.1007/s11547-025-02166-w.
[33] Jerman T, Pernus F, Likar B, et al. Enhancement of vascular structures in 3D and 2D angiographic images. IEEE Trans Med Imaging. 2016;35(9):2107–2118. doi:10.1109/TMI.2016.2550102.
[34] Pelosi P, Goldner M, McKibben A, et al. Recruitment and derecruitment during acute respiratory failure. Am J Respir Crit Care Med. 2001;164(1):122–130. doi:10.1164/ajrccm.164.1.2007010.
[35] Tavares V, Prata D, Ferreira HA. Comparing SPM12 and CAT12 segmentation pipelines: a brain tissue volume-based age and Alzheimer's disease study. J Neurosci Methods. 2020;334:108565. doi:10.1016/j.jneumeth.2019.108565.
[36] Peruzzo D, Bertoldo A, Zanderigo F, et al. Automatic selection of arterial input function on dynamic contrast-enhanced MR images. Comput Methods Programs Biomed. 2011;104(3):e148–e157. doi:10.1016/j.cmpb.2011.02.012.
[37] Boxerman JL, Schmainda KM, Weisskoff RM. Relative cerebral blood volume maps corrected for contrast agent extravasation significantly correlate with glioma tumor grade, whereas uncorrected maps do not. AJNR Am J Neuroradiol. 2006;27(4):859–867.
[38] Stanojevic S, Kaminsky DA, Miller MR, et al. ERS/ATS technical standard on interpretive strategies for routine lung function tests. Eur Respir J. 2022;60(1):2101499. doi:10.1183/13993003.01499-2021.
[39] Terribilli D, Schaufelberger MS, Duran FLS, et al. Age-related gray matter volume changes in the brain during non-elderly adulthood. Neurobiol Aging. 2011;32(2):354–368. doi:10.1016/j.neurobiolaging.2009.02.008.
[40] Kalpouzos G, Chételat G, Baron J-C, et al. Voxel-based mapping of brain gray matter volume and glucose metabolism profiles in normal aging. Neurobiol Aging. 2009;30(1):112–124. doi:10.1016/j.neurobiolaging.2007.05.019.
[41] Fujita S, Mori S, Onda K, et al. Characterization of brain volume changes in aging individuals with normal cognition using serial magnetic resonance imaging. JAMA Netw Open. 2023;6(6):e2318153. doi:10.1001/jamanetworkopen.2023.18153.
[42] Mahammedi A, Ramos A, Bargalló N, et al. Brain and lung imaging correlation in patients with COVID-19: Could the severity of lung disease reflect the prevalence of acute abnormalities on neuroimaging? A global multicenter observational study. AJNR Am J Neuroradiol. 2021;42(6):1008–1016. doi:10.3174/ajnr.A7072.
[43] Staab KR, McIntosh MJ, Puliyakote ASK, et al. Long COVID: lung pathophysiology and its relationship with cognitive dysfunction. Sci Rep. 2025;15(1):42595. doi:10.1038/s41598-025-26568-y.
[44] Østergaard L. SARS CoV-2 related microvascular damage and symptoms during and after COVID-19: consequences of capillary transit-time changes, tissue hypoxia and inflammation. Physiol Rep. 2021;9(3):e14726. doi:10.14814/phy2.14726.
[45] Mehboob R, von Kries JP, Ehsan K, et al. Role of endothelial cells and angiotensin converting enzyme-II in COVID-19 and brain damages post-infection. Front Neurol. 2023;14:1210194. doi:10.3389/fneur.2023.1210194.
[46] Churchill NW, Roudaia E, Chen JJ, et al. Effects of post-acute COVID-19 syndrome on the functional brain networks of non-hospitalized individuals. Front Neurol. 2023;14:1136408. doi:10.3389/fneur.2023.1136408.
[47] Ajaz S, McPhail MJ, Singh KK, et al. Mitochondrial metabolic manipulation by SARS-CoV-2 in peripheral blood mononuclear cells of patients with COVID-19. Am J Physiol Cell Physiol. 2021;320(1):C57–C65. doi:10.1152/ajpcell.00426.2020.
[48] Zhang T, Li Y, Pan L, et al. Brain-wide alterations revealed by spatial transcriptomics and proteomics in COVID-19 infection. Nat Aging. 2024;4(11):1598–1618. doi:10.1038/s43587-024-00730-z.
[49] Chen S, Lan Y, Li H, et al. Relationship between lung and brain injury in COVID-19 patients: a hyperpolarized 129Xe-MRI-based 8-month follow-up. Biomedicines. 2022;10(4):781. doi:10.3390/biomedicines10040781.
[50] Du Y, Zhao W, Huang S, et al. Two-year follow-up of brain structural changes in patients who recovered from COVID-19: a prospective study. Psychiatry Res. 2023;319:114969. doi:10.1016/j.psychres.2022.114969.
[51] Benedetti F, Palladini M, Paolini M, et al. Brain correlates of depression, post-traumatic distress, and inflammatory biomarkers in COVID-19 survivors: a multimodal magnetic resonance imaging study. Brain Behav Immun Health. 2021;18:100387. doi:10.1016/j.bbih.2021.100387.
[52] Díez-Cirarda M, Yus M, Gómez-Ruiz N, et al. Multimodal neuroimaging in post-COVID syndrome and correlation with cognition. Brain. 2023;146(5):2142–2152. doi:10.1093/brain/awac384.

[53] Rothstein TL. Cortical Grey matter volume depletion links to neurological sequelae in post COVID-19 'long haulers'. BMC Neurol. 2023;23(1):22. doi:10.1186/s12883-023-03049-1.
[54] Sanabria-Diaz G, Etter MM, Melie-Garcia L, et al. Brain cortical alterations in COVID-19 patients with neurological symptoms. Front Neurosci. 2022;16:992165. doi:10.3389/fnins.2022.992165.
[55] Ajčević M, Iscra K, Furlanis G, et al. Cerebral hypoperfusion in post-COVID-19 cognitively impaired subjects revealed by arterial spin labeling MRI. Sci Rep. 2023;13(1):5808. doi:10.1038/s41598-023-32275-3.